



Efficient hydrogen production by selective alcohol photoreforming on plasmonic photocatalyst comprising sandwiched Au nanodisks and TiO₂



Albert Chang^{a,1}, Wei-Shun Peng^{a,1}, I-Tai Tsai^a, Li-Fen Chiang^a, Chia-Min Yang^{a,b,*}

^a Department of Chemistry, National Tsing Hua University, Hsinchu, 30013, Taiwan

^b Frontier Research Center on Fundamental and Applied Sciences of Matters, National Tsing Hua University, Hsinchu, 30013, Taiwan

ARTICLE INFO

Keywords:

Alcohol photoreforming
Photocatalysis
Plasmonic photocatalyst
Zeolite nanosheets

ABSTRACT

A nanocomposite comprising gold nanodisks (Au NDs) and titanium dioxide (TiO₂) nanophases sandwiched between zeolite nanosheets was fabricated for hydrogen production by plasmonic photocatalytic reforming of methanol. The inter-sheet space between zeolite nanosheets served as nanoconfinement for forming the edge-attached domains of Au NDs/TiO₂. Benefiting from the anisotropic shape of Au NDs and their edge attachment with TiO₂, the nanocomposite exhibited superior photoactivity for visible light (> 400 nm)-driven photoreforming of methanol and the hydrogen production rate was ~24 times higher than that of the benchmark Au@P25 photocatalyst. Moreover, experimental results suggest that zeolite nanosheets effectively gated the access to the surface of Au NDs and allowed only methanol but not higher alcohols to react to produce hydrogen. Gradual deactivation was observed during methanol photoreforming, a phenomenon shown to be attributed to the chemisorbed CO accumulated on Au in the absence of oxygen.

1. Introduction

Intensive research has been focused on the plasmonic metal nanostructures mainly because of a renewed interest in the harvesting and conversion of solar energy [1–4]. Plasmonic metal nanostructures are characterized by their strong interactions with resonant photons to excite localized surface plasmon resonance (SPR) [5–7]. When coupled with a semiconducting material, the localized SPR may enhance the local electromagnetic fields around the semiconductor to generate electron-hole pairs for photocatalytic reactions [8,9]. The most frequently studied system is the combination of gold (Au) and titanium dioxide (TiO₂) for photocatalytic hydrogen (H₂) production or other reactions [10–13]. Anisotropic Au nanostructures such as Au nanorods (NRs) and Au nanodisks (NDs) exhibit size- and shape-dependent SPR absorption and manifest an efficient and wide range of light harvesting for photocatalysis [14,15]. It is recognized that the longitudinal SPR mode is the main channel for transferring the hot electrons from Au to TiO₂ [7], and therefore selective deposition of TiO₂ or other electron acceptors at the tip of Au NRs or at the edge of Au NDs results in highly active plasmonic photocatalysts [16]. For Au NDs, the SPR wavelength and the sensitivity of the wavelength to a change in surrounding refractive index have been shown to increase with increasing aspect ratio of Au NDs [15].

On the other hand, zeolites are crystalline microporous materials and can act as molecular sieves for size- and shape-selective adsorption and separation [17–19]. Recently, new strategy has been developed to synthesize ultrathin zeolite nanosheets using bifunctional structure-directing agents (SDAs) [20–22]. The discovery opens wide opportunity for innovative combination of zeolites with other types of materials for advanced applications. Herein we report a novel type of such nanocomposites for efficient visible light-driven photocatalytic H₂ production by size-exclusive alcohol photoreforming. Very recently, we designed a triblock SDA to synthesize hierarchical silicalite-1 (with MFI structure) octahedra comprising highly-branched and orthogonally-stacked plates of parallel and spaced zeolite nanosheets [23]. In this study, as shown in Fig. 1, we made use of the inter-sheet slit-type space between zeolite nanosheets for confined fabrication of edge-attached composites of Au NDs and TiO₂ by the co-impregnation of chloroauric acid (HAuCl₄) and ammonium titanyl oxalate ((NH₄)₂TiO(C₂O₄)₂). The electrostatic interactions between chloroauric anions (AuCl₄⁻) and titanyl cations (TiO²⁺) prevented possible sintering of Au [24], a problem often encountered by the noble metal [25], and ensured the entrapment of Au NDs and TiO₂ in the inter-sheet space after subsequent fabrication steps. The plasmonic photocatalysts exhibited superior activity for H₂ production by photoreforming of methanol. Moreover, the microporous silicalite-1 nanosheets effectively gated the access to the

* Corresponding author at: Department of Chemistry, National Tsing Hua University, Hsinchu, 30013, Taiwan.

E-mail address: cmyang@mx.nthu.edu.tw (C.-M. Yang).

¹ These authors contributed equally to this work.

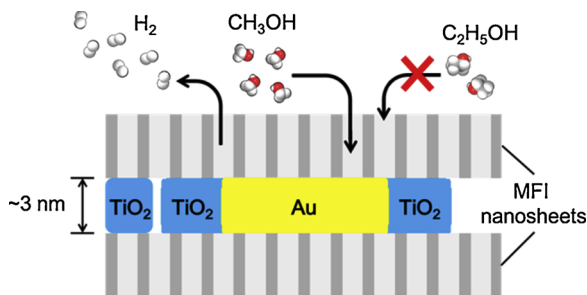


Fig. 1. Schematic representation of hydrogen production by selective alcohol photoreforming on Au/TiO₂@h-S.

surface of Au NDs and allowed only methanol but not ethanol or higher alcohols to react to produce H₂. For the first time, the combination of efficient plasmonic photocatalytic activity of anisotropic Au NDs and molecular sieving effect of zeolite nanosheets was demonstrated. The results show promise of such type of innovative nanocomposites for energy- and environment-related applications.

2. Experimental section

2.1. Materials preparation

2.1.1. Synthesis of hierarchical silicalite-1

The triblock SDA (C₆H₁₃–N⁺(CH₃)₂–C₆H₁₂–N⁺(CH₃)₂–C₆H₁₂–N⁺(CH₃)₂–(CH(CH₃)CH₂O)₆–N⁺(CH₃)₂–C₆H₁₂–N + (CH₃)₂–C₆H₁₂–N⁺(CH₃)₂–C₆H₁₃(6OH[–]), designated as N₃–PO₆–N₃, was synthesized by following similar procedures reported previously [23]. For the synthesis of the hierarchical silicalite-1 octahedra [23], N₃–PO₆–N₃ (0.2 mmol) was dissolved in the aqueous solution (7 mL) containing NaOH and H₂SO₄. Tetraethylorthosilicate (TEOS, 0.01 mol) was then added under vigorous stir, resulting in a mixture with molar composition of 50 SiO₂ : 1 N₃–PO₆–N₃ : 15 Na₂O : 9 H₂SO₄ : 2500 H₂O. The mixture was transferred to an autoclave to be heated at 150 °C for 2 days. The product was filtered and dried at 90 °C and was designated as h-S.

2.1.2. Preparation of nanocomposites with Au and TiO₂

The hierarchical silicalite-1 octahedra (h-S) was first stirred in aqueous solution of H₂SO₄ (45 wt%) at 95 °C for 1 day to decompose the PO block of the SDA and vacate the inter-sheet space [23]. After being repeatedly washed by water and acetone and was finally dried at 90 °C, the acid-treated h-S (0.1 g) was mixed with a solution (1.6 mL) of HCl (1.0 N) containing HAuCl₄·4H₂O (0.02 mmol) and (NH₄)₂TiO (C₂O₄)₂·H₂O (0.1 mmol). The mixture was stirred at room temperature for 1 h and then dried at room temperature in vacuum. The solid was heated in hydrogen flow at 200 °C for 3 h and finally calcined in air at 500 °C for 3 h to result in Au/5TiO₂@h-S. The reference sample Au/1TiO₂@h-S was prepared by the same procedures except that 0.02 mmol (instead of 0.1 mmol) of (NH₄)₂TiO(C₂O₄)₂·H₂O was used for the step of impregnation. The reference samples solely containing Au or TiO₂ (*i.e.* Au@h-S and TiO₂@h-S) were prepared by impregnation with a solution containing only HAuCl₄·4H₂O or (NH₄)₂TiO(C₂O₄)₂·H₂O followed by the same subsequent procedures. Au@P25 (with Au/Ti molar ratio of 1:240) was prepared by following the reported procedures [26]. Au/5TiO₂@SBA was prepared by the same procedures of Au/5TiO₂@h-S using mesoporous silica SBA-15 (synthesized by following the reported procedures [27]) instead of h-S as a support.

2.1.3. Materials characterization

X-ray diffraction (XRD) patterns were recorded on Bruker D8 diffractometer using Cu K α radiation. Scanning electron microscopy (SEM) and backscattered electrons-scanning electron microscopy (BSE-

SEM) images were obtained using a field emission JEOL JSM-7000 F microscope with a BSE detector operated at 10 kV. Nitrogen physisorption isotherms were measured at 77 K using a Quantachrome Autosorb-1-MP instrument. The pore size distribution was analyzed by nonlocal density functional theory (NLDFT) method using the kernel of NLDFT adsorption branch model. Inductively coupled plasma–mass spectroscopy (ICP-MS) results were obtained on a Perkin-Elmer SCIEX-ELAN5000 device. Transmission electron microscopy (TEM) images and energy dispersive X-ray spectroscopy (EDX) measurements were taken by a JEOL JEM-ARM200FTH microscope equipped with an energy dispersive X-ray spectrometer. DR UV-vis absorption spectra were recorded on a JASCO V-650 spectrophotometer equipped with an integrating sphere accessory ISV-722. Ti K-edge X-ray absorption near edge structure (XANES) spectrum was collected on the beamline 17C at the National Synchrotron Radiation Research Center (NSRRC, Taiwan) with a storage ring energy of 1.5 GeV.

2.1.4. Photocatalytic study

The experiments were carried out in a closed quartz reaction cell. A photocatalyst (0.02 g) was dispersed in 10 vol% aqueous solution (50 mL) of methanol (or ethanol, 1-propanol and 1-butanol). Before the irradiation started, the suspension was bubbled with Ar flow for 30 min to completely remove the dissolved O₂. The suspension was then irradiated by 500 W Hg-Xe arc lamp through a cut-off filter ($\lambda > 400$ nm). The evolved gases were analyzed by GC (Shimadzu GC-2014 with argon carrier gas, MS-5A column, and TCD detector). The mean H₂ evolution rate was determined by averaging the total amount of H₂ generated within 1 h. For the study on the influence of the presence of reaction intermediates on H₂ production, the 10 vol% aqueous solutions (50 mL) of methanol containing formaldehyde (1 M), formic acid (1 M) or carbon monoxide (by bubbling the gas for 1 h) were prepared. Au/5TiO₂@h-S (0.02 g) was then dispersed in each of the three solutions and the suspension was irradiated and analyzed by the same conditions as above mentioned. Prior to the addition of Au/5TiO₂@h-S, the solutions containing formaldehyde or formic acid were bubbled with Ar flow for 30 min to remove the dissolved O₂.

3. Results and discussion

The zeolitic structure of silicalite-1 octahedra h-S and its unique hierarchical architecture of highly-branched and orthogonally-stacked zeolite nanoplates were confirmed by XRD and SEM, respectively (Fig. S1). The inter-sheet space (~3 nm) was vacated by sulfuric acid treatment [23,28,29] (cf. nitrogen physisorption isotherm and pore size distribution in Fig. S2) and was then impregnated by an acidified solution of chloroauric acid and ammonium titanyl oxalate with an Au-to-Ti molar ratio of 1:5. The mixture was dried and then heated in H₂ flow to reduce Au and finally calcined to fully decompose the titanium precursor to form TiO₂. ICP-MS analysis indicated that the Au loading of the resulting nanocomposite, designated as Au/5TiO₂@h-S, was ~4.2 wt% and that the actual Au-to-Ti molar ratio was nearly identical to the nominal value (cf. Table S1 for ICP-MS results). The BSE-SEM revealed that the reduced Au particles were small and highly dispersed in Au/5TiO₂@h-S (cf. Fig. 2a). No large Au particles on the external surface of the hierarchical silicalite-1 were observed. In line with the observation, the XRD pattern of Au/5TiO₂@h-S contained reflections of metallic Au that are relatively wide (cf. Fig. 2a, marked by asterisks). The average crystalline domain size of Au is estimated to be 9 nm from the width of Au(111) reflection by the Scherrer equation (see supplementary information for detailed estimation), assuming spherical shape of Au [24,25,27]. In contrast, the reference sample containing only Au (Au@h-S) showed relatively intense and sharp X-ray reflections of Au and large Au particles on the external surface of hierarchical silicalite-1 were observed (cf. Fig. S4). The results revealed the crucial role of the electrostatic interactions between chloroauric anions and titanyl cations in suppressing the migration of Au species from the inter-

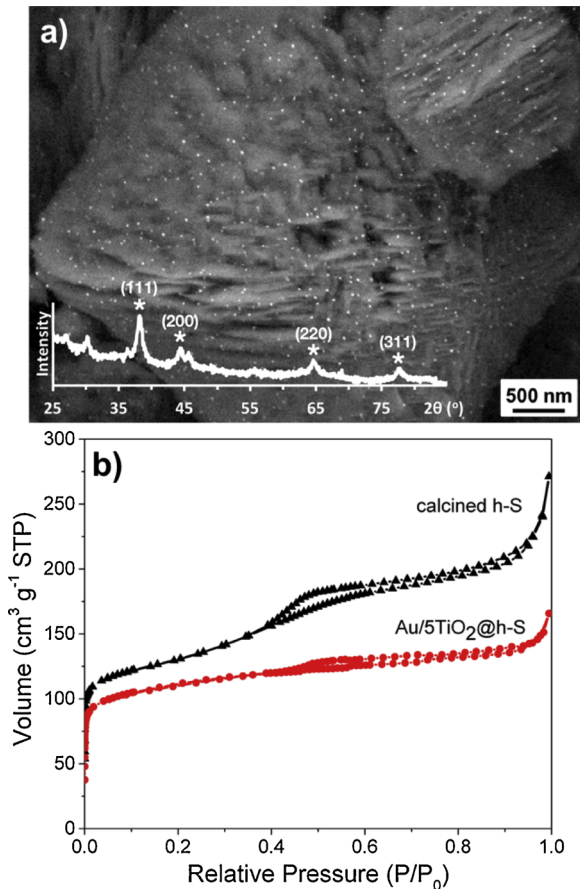


Fig. 2. (a) BSE-SEM image and XRD pattern of Au/5TiO₂@h-S. The peaks marked by asterisks are attributed to metallic Au. (b) Comparison of nitrogen physisorption isotherms of Au/5TiO₂@h-S and calcined h-S.

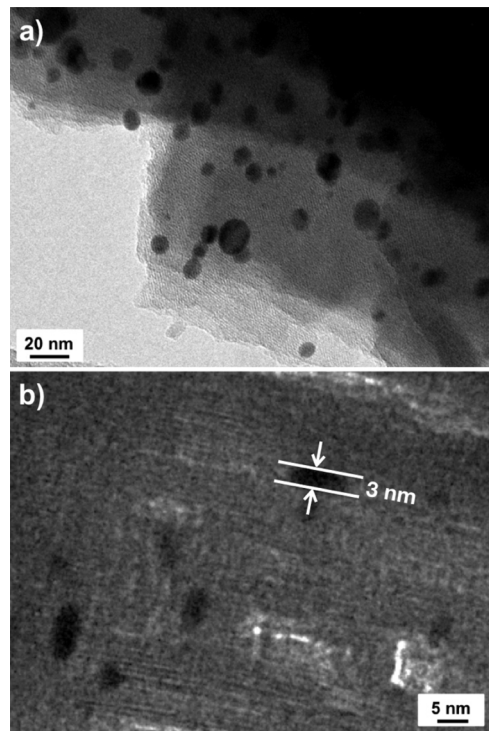


Fig. 3. TEM images of Au/5TiO₂@h-S viewed (a) perpendicular to or (b) along the *a-c* planes of silicalite-1 nanosheets.

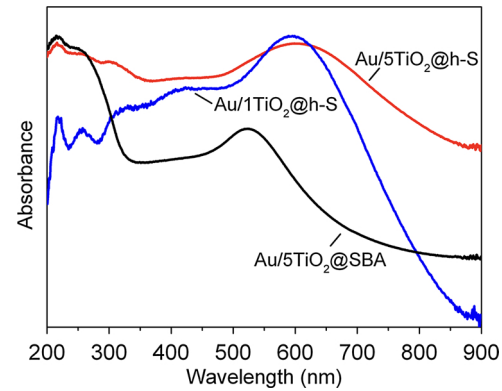


Fig. 4. Comparison of DR UV-vis spectra of Au/5TiO₂@h-S, Au/1TiO₂@h-S and Au/5TiO₂@SBA.

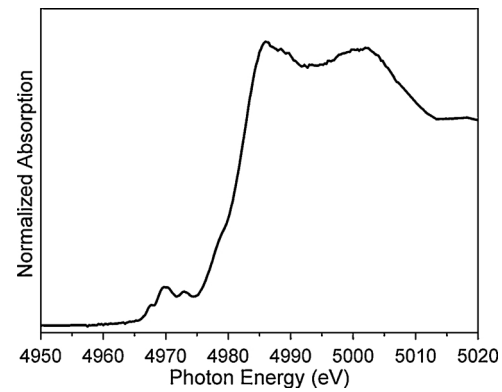


Fig. 5. Ti K-edge XANES spectrum of Au/5TiO₂@h-S.

sheet space during preparation steps [24,30].

The presence of the micropores of silicalite-1 nanosheets was confirmed by nitrogen physisorption analysis (cf. Fig. 2b), and the micropore volume of the calcined h-S was calculated to be $0.16 \text{ cm}^3 \text{ g}_{\text{SiO}_2}^{-1}$. The micropore volume of Au/5TiO₂@h-S was $0.13 \text{ cm}^3 \text{ g}_{\text{sample}}^{-1}$, which could be converted to $0.15 \text{ cm}^3 \text{ g}_{\text{SiO}_2}^{-1}$ considering only the weight of silicalite-1 (instead of total weight of silicalite-1 plus Au and TiO₂, calculated based on ICP-MS results shown in Table S1). The value is nearly identical to the micropore volume of the calcined h-S ($0.16 \text{ cm}^3 \text{ g}_{\text{SiO}_2}^{-1}$), suggesting that the micropores of silicalite-1 nanosheets were not filled or completely blocked by Au and TiO₂. In addition, the analyses of the isotherms of Au/5TiO₂@h-S, the calcined h-S and acid-treated h-S (Fig. S2), suggested that the Au and TiO₂ were mainly deposited in the inter-sheet space to cause a diminishment of the H4-type hysteresis loop (at a relative pressure of 0.4–0.8) that was partially attributed to the inter-sheet porosity of the hierarchical silicalite-1 [23]. Moreover, the TEM images of the crushed sample viewed perpendicular to or along the *a-c* planes of silicalite-1 nanosheets confirmed the confined growth of Au NDs in the inter-sheet space (cf. Fig. 3). The Au NDs had thicknesses of ~3 nm, corresponding well to the inter-sheet space (indicated by arrows), and diameters of 5–20 nm. The wide diameter distribution of Au NDs also explained the broadband absorption of Au/5TiO₂@h-S in the visible light region (cf. Fig. 4). On the other hand, X-ray absorption spectroscopy was further applied to analyze the titanium species in the nanocomposite since they could not be identified by TEM due to low image contrast correlating with the atomic number of constituent elements. EDX analysis was also conducted to confirm that the Au-to-Ti and Ti-to-Si molar ratios were very close to the nominal values, but the intensity of the signals attributed to Ti was too low to perform elemental mapping in the TEM image. As shown in Fig. 5, the Ti K-edge XANES spectrum of Au/5TiO₂@h-S contained three weak pre-edge peaks at 4965–4975 eV, which are

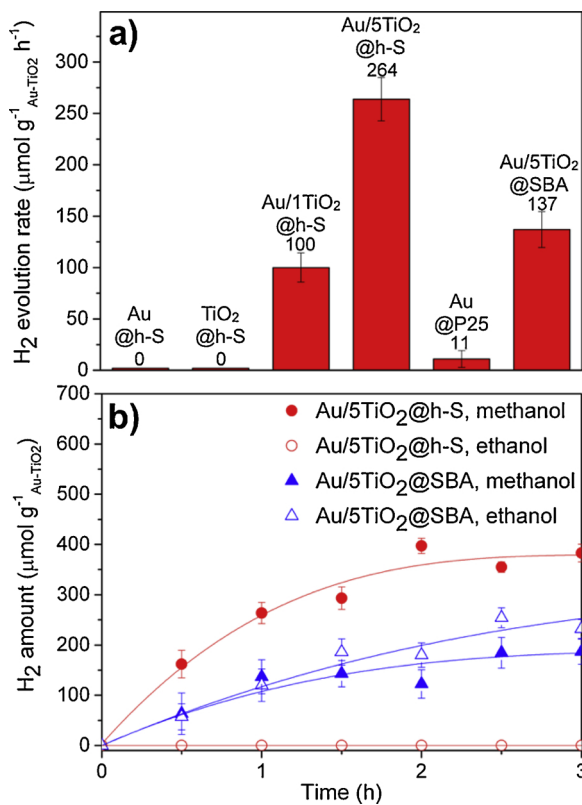


Fig. 6. (a) Comparison of the mean H_2 evolution rates from 10 vol% aqueous solution of methanol by selected samples. (b) Overall H_2 production in 10 vol% aqueous solution of methanol or ethanol by Au/5TiO₂@h-S or Au/5TiO₂@SBA.

characteristic of octahedrally-coordinated Ti^{4+} species of bulk TiO_2 [31]. This implicates that the titanium species were “aggregated” to form XRD-amorphous TiO_2 nanophases in the inter-sheet space of hierarchical silicalite-1.

The nanocomposite Au/5TiO₂@h-S and reference samples were applied as catalysts for photoreforming of methanol under visible light irradiation ($> 400 \text{ nm}$, with a 500 W Hg-Xe arc lamp through a cut-off filter). Fig. 6a compares the mean H_2 evolution rates from 10 vol% aqueous solution of methanol determined by averaging the total amount of H_2 generated within 1 h. Au/5TiO₂@h-S exhibited superior photoactivity and produced $264 \mu\text{mol g}^{-1} \text{Au-TiO}_2 \text{ h}^{-1}$. The activity was ~ 24 times higher than the value ($11 \mu\text{mol g}^{-1} \text{Au-TiO}_2 \text{ h}^{-1}$) of the Au catalyst supported on Degussa P25 titania (Au@P25, containing 2–3 nm Au nanoparticles, cf. Fig. S5) and was about twice higher than the activity ($137 \mu\text{mol g}^{-1} \text{Au-TiO}_2 \text{ h}^{-1}$) of the reference sample containing the same loadings of Au and TiO_2 on mesoporous silica SBA-15 (Au/5TiO₂@SBA, containing 6–7 nm Au nanoparticles in 7 nm-wide mesopores, cf. Fig. S6). For the hierarchical silicalite-1-supported reference samples solely containing Au or TiO_2 (i.e. Au@h-S and TiO_2 @h-S), no H_2 was detected at all. With Au@P25 as a benchmark photocatalyst for comparison, the photoactivity of Au/5TiO₂@h-S was superior than most reported plasmonic photocatalysts based on composites of TiO_2 and Au NRs or other Au nanostructures [16,32,33]. The high plasmonic photoactivity of Au/5TiO₂@h-S strongly supports that plenty of the edge-attached Au/TiO₂ domains were present in the nanocomposite so as to facilitate the transfer of the electrons generated by the localized longitudinal SPR on Au NDs to TiO_2 nanophases upon visible light irradiation. This could also explain the fact that the reference sample prepared with Au-to-Ti molar ratio of 1:1 (designated as Au/1TiO₂@h-S) exhibited much lower activity ($100 \mu\text{mol/g}_{\text{Au-TiO}_2}$) than Au/5TiO₂@h-S did, because the more the Au NDs were attached by TiO_2 , the higher the efficiency of Au-to-TiO₂ electron transfer was and therefore the higher the photocatalytic

activity became. Additional evidence of the formation of edge-attached Au/TiO₂ domains came from the diffuse reflectance (DR) UV-vis absorption spectra of the two samples. The SPR absorption band was redshifted with increasing the relative amount of TiO_2 (cf. Fig. 4). The phenomenon could be explained by the influence of the dielectric constant of the surrounding medium of Au NDs [5], and the more the Au NDs were surrounded and attached by TiO_2 , the higher the effective value of the surrounding’s dielectric constant became and therefore the more redshift was observed.

In the reaction of H_2 production by methanol photoreforming, it is generally recognized that methanol gets oxidized by the photo-generated holes while water is the source of hydrogen and receives photogenerated electrons to produce H_2 . Recently, Waterhouse and coworkers have studied the photocatalytic activities of several photocatalysts for H_2 production in various alcohol-water mixtures (0–100 vol%) [34]. They found that H_2 could be produced in pure methanol and other alcohols, but the rate of H_2 production in pure methanol was much lower than those in aqueous solutions of methanol [34]. To see if similar phenomena also took place for our nanocomposite photocatalyst, we conducted the visible light-driven reactions in pure water and pure methanol under otherwise the same conditions. Interestingly, we found that while no H_2 was measured in pure water, production of H_2 was observed in pure methanol with a rate of $193 \mu\text{mol g}^{-1} \text{Au-TiO}_2 \text{ h}^{-1}$, around 73% of that conducted in 10 vol% aqueous solution of methanol (i.e. $264 \mu\text{mol g}^{-1} \text{Au-TiO}_2 \text{ h}^{-1}$). The results confirmed that methanol could serve as a hydrogen source to receive the photogenerated electrons and produce H_2 . Nevertheless, for the reaction conducted in 10 vol% aqueous solution of methanol, water is the solvent and can dissociate to produce protons (or hydronium ions) that are much smaller and diffuse much faster than methanol to get reduced to form H_2 on the surface of TiO_2 .

In Au/5TiO₂@h-S, the edge-attached Au/TiO₂ domains were sandwiched between silicalite-1 nanosheets. As a result, the Au NDs could be accessible mainly through the straight micropores (with a dimension of $5.4 \times 5.6 \text{ \AA}$ [35]) of the nanosheets. To examine the molecular sieving effect of the zeolitic nanosheets, we conducted the visible light-driven photoreforming of methanol and higher alcohols and compared the time courses of H_2 evolution catalyzed by Au/5TiO₂@h-S and a reference sample Au/5TiO₂@SBA (cf. Fig. 6b). For the reaction with methanol, as aforementioned, Au/5TiO₂@h-S produced around twice the amount of H_2 than Au/5TiO₂@SBA did. The accumulated amounts of H_2 for both samples did not further increase after two hours of irradiation, indicating that the photocatalysts were deactivated during the reactions. Similar phenomenon of deactivation has been previously reported for different types of Au-TiO₂ photocatalysts [16,32]. When methanol was replaced by ethanol, interestingly, nearly the same amount of H_2 (as in the case of methanol) was produced by Au/5TiO₂@SBA but no H_2 was detected in the case of Au/5TiO₂@h-S. No H_2 was produced photocatalytically from 1-propanol or 1-butanol with Au/5TiO₂@h-S, either. The observed “sieving” effect for Au/5TiO₂@h-S could be comprehended by considering the diffusivities of water, methanol and ethanol in silicalite-1 [17]. Even though the three molecules are slightly different in size but are all small enough [36] to enter the micropores of silicalite-1, water diffuses significantly faster than ethanol in silicalite-1 [17]. Therefore, for the reaction with 10 vol% aqueous solution of ethanol, the accessibility of Au NDs for ethanol molecules through the sandwiching zeolite nanosheets was markedly lowered by water molecules that was present in relatively large amount. Such a situation would not take place in the case of Au/5TiO₂@SBA, a photocatalyst with higher accessibility of Au nanoparticles through much wider (7 nm) diffusion path.

As aforementioned, Au/5TiO₂@h-S and Au/5TiO₂@SBA were deactivated after prolonged reaction of visible light-driven photoreforming of methanol. Although similar phenomenon has been observed for other Au-TiO₂ photocatalysts [16,32], possible causes remain unclear. We speculate that it might be attributed to the blocking of

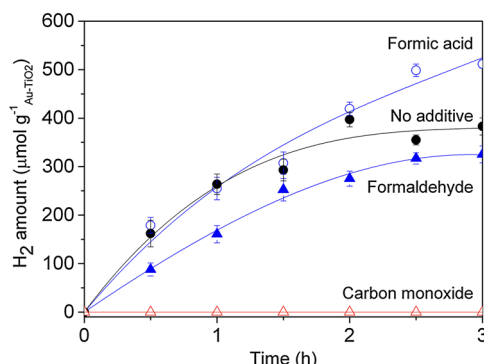


Fig. 7. Overall H₂ production in 10 vol% aqueous solution of methanol by Au/5TiO₂@h-S with the presence of formaldehyde, formic acid or carbon monoxide.

catalytically active sites on Au NDs by the adsorption of some by-products or intermediates of the reaction. Molecules including formaldehyde, formic acid and carbon monoxide are key intermediates during the photoreforming of methanol [37], and we tested their possible influences on the photocatalytic activity of Au/5TiO₂@h-S by conducting the reactions in the 10 vol% aqueous solutions of methanol that simultaneously contained formaldehyde (1 M), formic acid (1 M) or carbon monoxide (CO, bubbled for 1 h). As shown in Fig. 7, the presence of formaldehyde or formic acid resulted in opposite effect on H₂ production, with the former slightly suppressing but the latter slightly enhancing (after 1 h irradiation) the production. On the contrary, no H₂ was detected when CO was purged into the O₂-free reaction mixture. Obviously, the presence of CO should be responsible for the deactivation of Au/5TiO₂@h-S and other Au-TiO₂ photocatalysts during photoreforming of methanol. It is known that CO exhibits great affinity to be chemically adsorbed on metallic Au [38]. In the absence of O₂, the accumulated chemisorbed CO molecules could not be further oxidized to carbon dioxide [39] and may eventually block the surface of Au to deactivate the photocatalysts. Similar deactivation tendency was observed in the oxidation of CO on a zirconia-supported Au catalyst [39]. The suppression of H₂ production by formaldehyde has been previously observed [40] and is likely to be associated to the fact that the molecule can be split photocatalytically relatively easily to produce H₂ accompanying with the formation of CO as a byproduct [41] to deactivate the Au-TiO₂ photocatalysts. As for the positive effect of formic acid, it could be understood by considering the fact that it is easier for formic acid to be photocatalytically decomposed to form H₂ (and carbon dioxide) than methanol and formaldehyde [26,40].

4. Conclusions

A successful combination of plasmonic photocatalyst and zeolite nanosheets has been demonstrated. The use of inter-sheet space between zeolite nanosheets in the hierarchical silicalite-1 octahedra realizes the confined fabrication of edge-attached domains of Au nanodisks and TiO₂ nanophases. The resulting nanocomposite not only exhibits high visible light-driven photocatalytic activity for hydrogen production by photoreforming of methanol, but also shows molecular sieving capability for allowing methanol but not higher alcohols to be reformed. The photocatalytic performance is much better than the benchmark Au@P25 photocatalyst, and the observed gradual deactivation may be attributed to the accumulation of the chemisorbed CO molecules on the Au surface.

Acknowledgements

The authors gratefully acknowledge the financial supports of the Ministry of Science and Technology, Taiwan under the contracts No.

MOST 106-2113-M-007-025-MY3 and MOST 107-3017-F-007-002. This study was also supported by the Frontier Research Center on Fundamental and Applied Sciences of Matters from The Featured Areas Research Center Program within the framework of the Higher Education Sprout Project by the Ministry of Education (MOE) in Taiwan.

Appendix A. Supplementary data

Supplementary material related to this article can be found, in the online version, at doi:<https://doi.org/10.1016/j.apcatb.2019.117773>.

References

- [1] S. Linic, P. Christopher, D.B. Ingram, Plasmonic-metal nanostructures for efficient conversion of solar to chemical energy, *Nat. Mater.* 10 (2011) 911–921.
- [2] S. Sarina, E.R. Waclawik, H. Zhu, Photocatalysis on supported gold and silver nanoparticles under ultraviolet and visible light irradiation, *Green Chem.* 15 (2013) 1814–1833.
- [3] X.-C. Ma, Y. Dai, L. Yu, B.-B. Huang, Energy transfer in plasmonic photocatalytic composites, *Light-Sci. Appl.* 5 (2016) e16017.
- [4] Y. Zhang, S. He, W. Guo, Y. Hu, J. Huang, J.R. Mulcahy, W.D. Wei, Surface-plasmon-driven hot electron photochemistry, *Chem. Rev.* 118 (2018) 2927–2954.
- [5] X.M. Zhang, Y.L. Chen, R.S. Liu, D.P. Tsai, Plasmonic photocatalysis, *Rep. Prog. Phys.* 76 (2013) 046401.
- [6] Z. Zheng, T. Tachikawa, T. Majima, Single-particle study of Pt-modified Au nanorods for plasmon-enhanced hydrogen generation in visible to near-infrared region, *J. Am. Chem. Soc.* 136 (2014) 6870–6873.
- [7] Z. Lou, M. Fujitsuka, T. Majima, Pt–Au triangular nanoprisms with strong dipole plasmon resonance for hydrogen generation studied by single-particle spectroscopy, *ACS Nano* 10 (2016) 6299–6305.
- [8] D.A. Panayotov, J.R. Morris, Surface chemistry of Au/TiO₂: thermally and photo-activated reactions, *Surf. Sci. Rep.* 71 (2016) 77–271.
- [9] B. Gupta, A.A. Melvin, T. Matthews, S. Dash, A.K. Tyagi, TiO₂ modification by gold (Au) for photocatalytic hydrogen (H₂) production, *Renew. Sust. Energ. Rev.* 58 (2016) 1366–1375.
- [10] X.Y. Cai, M.S. Zhu, O.A. Elbanna, M. Fujitsuka, S. Kim, L. Mao, J.Y. Zhang, T. Majima, Au nanorod photosensitized La₂Ti₂O₇ nanosteps: successive surface heterojunctions boosting visible to near-infrared photocatalytic H-2 evolution, *ACS Catal.* 8 (2018) 122–131.
- [11] Y.L. Si, S. Cao, Z.J. Wu, Y.L. Ji, Y. Mi, X.C. Wu, X.F. Liu, L.Y. Piao, What is the predominant electron transfer process for Au NRs/TiO₂ nanodumbbell heterostructure under sunlight irradiation? *Appl. Catal. B-Environ.* 220 (2018) 471–476.
- [12] A. Zielinska-Jurek, E. Kowalska, J.W. Sobczak, W. Lisowski, B. Ohtani, A. Zaleska, Preparation and characterization of monometallic (Au) and bimetallic (Ag/Au) modified-titania photocatalysts activated by visible light, *Appl. Catal. B-Environ.* 101 (2011) 504–514.
- [13] V. Vaiano, G. Iervolino, D. Sannino, J.J. Murcia, M.C. Hidalgo, P. Ciambelli, J.A. Navio, Photocatalytic removal of patent blue V dye on Au-TiO₂ and Pt-TiO₂ catalysts, *Appl. Catal. B-Environ.* 188 (2016) 134–146.
- [14] S. Link, M.A. El-Sayed, Optical properties and ultrafast dynamics of metallic nanocrystals, *Annu. Rev. Phys. Chem.* 54 (2003) 331–366.
- [15] P. Hanarp, M. Käll, D.S. Sutherland, Optical properties of short range ordered arrays of nanometer gold disks prepared by colloidal lithography, *J. Phys. Chem. B* 107 (2003) 5768–5772.
- [16] B.H. Wu, D.Y. Liu, S. Mubeen, T.T. Chuong, M. Moskovits, G.D. Stucky, Anisotropic growth of TiO₂ onto gold nanorods for plasmon-enhanced hydrogen production from water reduction, *J. Am. Chem. Soc.* 138 (2016) 1114–1117.
- [17] T.C. Bowen, R.D. Noble, J.L. Falconer, Fundamentals and applications of pervaporation through zeolite membranes, *J. Membr. Sci.* 245 (2004) 1–33.
- [18] N.W. Ockwig, T.M. Nenoff, Membranes for hydrogen separation, *Chem. Rev.* 107 (2007) 4078–4110.
- [19] M. Yu, R.D. Noble, J.L. Falconer, Zeolite membranes: microstructure characterization and permeation mechanisms, *Accounts Chem. Res.* 44 (2011) 1196–1206.
- [20] M. Choi, K. Na, J. Kim, Y. Sakamoto, O. Terasaki, R. Ryoo, Stable single-unit-cell nanosheets of zeolite MFI as active and long-lived catalysts, *Nature* 461 (2009) 246–249.
- [21] K. Na, M. Choi, W. Park, Y. Sakamoto, O. Terasaki, R. Ryoo, Pillared MFI zeolite nanosheets of a single-unit-cell thickness, *J. Am. Chem. Soc.* 132 (2010) 4169–4177.
- [22] K. Na, C. Jo, J. Kim, K. Cho, J. Jung, Y. Seo, R.J. Messinger, B.F. Chmelka, R. Ryoo, Directing zeolite structures into hierarchically nanoporous architectures, *Science* 333 (2011) 328–332.
- [23] A. Chang, H.M. Hsiao, T.H. Chen, M.W. Chu, C.M. Yang, Hierarchical silicalite-1 octahedra comprising highly-branched orthogonally-stacked nanoplates as efficient catalysts for vapor-phase Beckmann rearrangement, *Chem. Commun. (Camb.)* 52 (2016) 11939–11942.
- [24] S.-P. Huang, C.-Y. Lin, H.-A. Chen, C.-M. Yang, An “Ion pairing” strategy for facile fabrication of densely packed gold nanostructures in ordered mesoporous silicas, *Microporous Mesoporous Mater.* 284 (2019) 53–59.
- [25] C.-M. Yang, H.-S. Sheu, K.-J. Chao, Templated synthesis and structural study of

densely packed metal nanostructures in MCM-41 and MCM-48, *Adv. Funct. Mater.* 12 (2002) 143–148.

[26] C. Gomes Silva, R. Juárez, T. Marino, R. Molinari, H. García, Influence of excitation wavelength (UV or visible light) on the photocatalytic activity of titania containing gold nanoparticles for the generation of hydrogen or oxygen from water, *J. Am. Chem. Soc.* 133 (2011) 595–602.

[27] C.-H. Liu, Y. Guan, E.J.M. Hensen, J.-F. Lee, C.-M. Yang, Au/TiO₂@SBA-15 nanocomposites as catalysts for direct propylene epoxidation with O₂ and H₂ mixtures, *J. Catal.* 282 (2011) 94–102.

[28] C.-M. Yang, B. Zibrowius, W. Schmidt, F. Schüth, Stepwise removal of the copolymer template from mesopores and micropores in SBA-15, *Chem. Mater.* 16 (2004) 2918–2925.

[29] C.-M. Yang, B. Zibrowius, W. Schmidt, F. Schüth, Consecutive generation of mesopores and micropores in SBA-15, *Chem. Mater.* 15 (2003) 3739–3741.

[30] T. Otto, S.I. Zones, E. Iglesia, Challenges and strategies in the encapsulation and stabilization of monodisperse Au clusters within zeolites, *J. Catal.* 339 (2016) 195–208.

[31] K. Ikeue, S. Ikeda, A. Watanabe, B. Ohtani, Elucidation of the local structure of active titanium(IV) sites on silica-based phase-boundary catalysts for alkene epoxidation with aqueous hydrogen peroxide, *Phys. Chem. Chem. Phys.* 6 (2004) 2523–2528.

[32] Z.W. Seh, S. Liu, M. Low, S.-Y. Zhang, Z. Liu, A. Mlayah, M.-Y. Han, Janus Au-TiO₂ photocatalysts with strong localization of plasmonic near-fields for efficient visible-light hydrogen generation, *Adv. Mater.* 24 (2012) 2310–2314.

[33] B. Liu, Y. Jiang, Y. Wang, S.X. Shang, Y.M. Ni, N. Zhang, M.H. Cao, C.W. Hu, Influence of dimensionality and crystallization on visible-light hydrogen production of Au@TiO₂ core-shell photocatalysts based on localized surface plasmon resonance, *Catal. Sci. Technol.* 8 (2018) 1094–1103.

[34] W.-T. Chen, A. Chan, D. Sun-Waterhouse, J. Llorca, H. Idriss, G.I.N. Waterhouse, Performance comparison of Ni/TiO₂ and Au/TiO₂ photocatalysts for H₂ production in different alcohol-water mixtures, *J. Catal.* 367 (2018) 27–42.

[35] D.H. Olson, G.T. Kokotailo, S.L. Lawton, W.M. Meier, Crystal structure and structure-related properties of ZSM-5, *J. Phys. Chem.* 85 (1981) 2238–2243.

[36] J.O. Hirschfelder, C.F. Curtiss, R.B. Bird, *Molecular Theory of Gases and Fluids*, John Wiley & Sons, Inc., New York City, 1954.

[37] G.L. Chiarello, M.H. Aguirre, E. Selli, Hydrogen production by photocatalytic steam reforming of methanol on noble metal-modified TiO₂, *J. Catal.* 273 (2010) 182–190.

[38] J. Gong, C.B. Mullins, Surface science investigations of oxidative chemistry on gold, *Accounts Chem. Res.* 42 (2009) 1063–1073.

[39] P. Konova, A. Naydenov, T. Tabakova, D. Mehandjiev, Deactivation of nanosize gold supported on zirconia in CO oxidation, *Catal. Commun.* 5 (2004) 537–542.

[40] A. Patsoura, D.I. Kondarides, X.E. Verykios, Photocatalytic degradation of organic pollutants with simultaneous production of hydrogen, *Catal. Today* 124 (2007) 94–102.

[41] E.S. Ranganathan, S.K. Bej, L.T. Thompson, Methanol steam reforming over Pd/ZnO and Pd/CeO₂ catalysts, *Appl. Catal. A-Gen.* 289 (2005) 153–162.